Controlling the bound states in a quantum-dot hybrid nanowire

Andrzej Ptok,[1,2,*] Aksel Kobiałka,[2,†] and Tadeusz Domański[2,‡]

[1]*Institute of Nuclear Physics, Polish Academy of Sciences, ul. E. Radzikowskiego 152, PL-31342 Kraków, Poland*

[2]*Institute of Physics, Marie Curie-Skłodowska University, pl. Marii Skłodowskiej-Curie 1, PL-20031 Lublin, Poland*

(Received 10 August 2017; published 22 November 2017)

Recent experiments using the quantum dot coupled to the topological superconducting nanowire [Deng *et al.*, Science **354**, 1557 (2016)] revealed that the zero-energy bound state coalesces from the Andreev bound states. Such quasiparticle states, present in the quantum dot, can be controlled by magnetic and electrostatic means. We use a microscopic model of the quantum-dot–nanowire structure to reproduce the experimental results, applying the Bogoliubov–de Gennes technique. This is done by studying the gate voltage dependence of the various types of bound states and mutual influence between them. We show that the zero-energy bound states can emerge from the Andreev bound states in the topologically trivial phase and can be controlled using various means. In the nontrivial topological phase we show the possible resonance between these zero-energy levels with Majorana bound states. We discuss and explain this phenomenon as a result of dominant spin character of discussed bound states. Presented results can be applied in experimental studies by using the proposed nanodevice.

DOI: 10.1103/PhysRevB.96.195430

I. EXPERIMENTAL INTRODUCTION

Boundaries of the low-dimensional topological superconductors can host the zero-energy Majorana bound states (MBS) [1–3]. Topological protection and non-Abelian statistics obeyed by such exotic quasiparticles make them appealing candidates for realization of stable qubits which could be useful for quantum computing [4–10]. Intensive studies of the topological superconductors provided evidence for the MBS in various nanodevices [11–24] which are tunable by the gate potentials and magnetic field, as have been demonstrated by Deng *et al.* in Ref. [24].

In practice the topologically nontrivial phase can be induced in nanoscopic systems via the superconducting proximity effect in cooperation with some additional effects, e.g., the spin-orbit coupling (SOC) and Zeeman splitting for semiconducting nanowires [20,21]. Such phenomena have been indeed reported for InAs-Al semiconductor-superconductor nanostructures [21] or at the interface between the semiconducting InSb nanowire and the NbTiN superconductor [23]. Another possible setup for this phenomenon is a nanowire with a proximity induced superconducting gap, due to the adatom deposition on a surface of the superconductor [25]. This has been reported, i.e., in the case of Fe [19,26] or Co [27] atoms on the Pb surface.

The Andreev bound states (ABSs) induced in the nanowire spectrum can be varied by the external magnetic field [28,29]. In some range of parameters [30–32], the above critical magnetic field transition from trivial to nontrivial topological phase occurs. One pair of such ABS merges at zero energy, giving rise to the (double degenerate) MBS, which is localized near the nanowire ends.

Recent experimental results of the Copenhagen group [24], showed that the ABS/MBS can be induced in a controllable way in the quantum-dot region side-coupled to the semiconductor-superconductor hybrid nanowire. A schematic of this structure is displayed in Fig. 1. The semiconducting InAs wire was epitaxially covered by the conventional Al superconductor [33], except for a small piece of wire which was interpreted as the quantum dot (QD). The thickness of the superconducting shell should be comparable to its coherence length, as some nontrivial finite-size effects can occur if this condition is not met [34]. Upon varying the magnetic field and the gate potential there have been induced the bound states of either the Andreev (Shiba) or the exotic Majorana type, as shown by peaks in the differential conductance of the tunneling current [35–37]. In particular, the QD energy levels can be varied by the gate voltage eventually leading to emergence of the zero-energy Majorana mode.

The main purpose of this paper is to explore the Andreev and Majorana bound states of the single and multiple quantum dots coupled to the hybrid nanowire. We study their evolution with respect to the electrostatic (gate) potential, magnetic field, and the chemical potential. This paper is organized as follows. In Sec. II we introduce the model and present some computational details concerning the Bogoliubov–de Gennes technique.

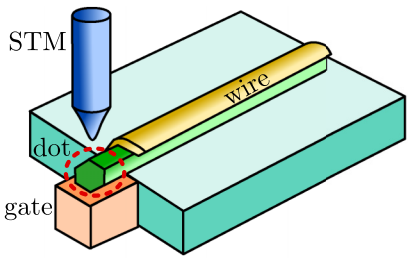

FIG. 1. Schematic representation of the experimental system discussed in Ref. [24]. InAs wire (green) is epitaxially covered by the superconducting Al (yellow). The quantum dot (InAs) is formed between the normal contact (dark orange) and the epitaxial Al shell (inside dashed circle). Magnetic field applied parallel to the wire axis can control the bound states. Measurements of the differential conductance have been done using the STM tip (blue), whereas the quantum-dot energy levels have been tuned by the gate potential.

*aptok@mmj.pl
†akob@kft.umcs.lublin.pl
‡doman@kft.umcs.lublin.pl

Next, in Sec. III we describe basic properties and main terminology in relation to the studied problem. Thorough discussion of the quasiparticle spectrum of the single QD is presented in Sec. IV. Revision of a more general system with a higher number of sites in QD, is performed in Secs. V and VI, which are devoted to the double and multisite QD cases, respectively. In Sec. VII we propose a feasible quantum device, which could enable an experimental realization of various tunable bound states. Finally, in Sec. VIII we summarize the results.

II. MODEL AND METHODS

For description of the nanostructure shown in Fig. 1, we will use a microscopic model in real space with Hamiltonian $\mathcal{H} = \mathcal{H}_w + \mathcal{H}_{\rm prox} + \mathcal{H}_{\rm soc} + \mathcal{H}_{\rm dot}$. The first term describes mobile electrons in the wire,

$$\mathcal{H}_w = \sum_{ij\sigma}\{-t\delta_{\langle i,j\rangle} - (\mu+\sigma h)\delta_{ij}\}c^\dagger_{i\sigma}c_{j\sigma}, \tag{1}$$

where t denotes a hopping integral between the nearest-neighbor sites, μ is a chemical potential, and h denotes a magnetic field parallel to the whole wire. Here $c^\dagger_{i\sigma}$ ($c_{i\sigma}$) describes the creation (annihilation) operator in site ith with spin σ. The second term accounts for the proximity effect,

$$\mathcal{H}_{\rm prox} = \sum_i \Delta(c_{i\downarrow}c_{i\uparrow} + c^\dagger_{i\uparrow}c^\dagger_{i\downarrow}), \tag{2}$$

and we assume the uniform energy gap Δ induced by the epitaxially covered classical superconductor. The spin-orbit coupling (SOC) term is given by

$$\mathcal{H}_{\rm soc} = -i\lambda\sum_{i\sigma\sigma'} c^\dagger_{i\sigma}(\sigma_y)_{\sigma\sigma'}c_{i+1,\sigma'}, \tag{3}$$

where σ_y stands for the y component of the Pauli matrix and λ is the SOC coupling along the chain. Then we treat the QD as part of a nanowire not covered by the superconductor. The last part,

$$\mathcal{H}_{\rm dot} = \sum_{i\in{\rm dot},\sigma} V_g c^\dagger_{i\sigma}c_{i\sigma}, \tag{4}$$

describes the electrostatic energy contributed by the gate potential V_g (see Fig. 2). In what follows we shall consider the quantum-dot region comprising one, two, and multiple sites coupled to the superconducting nanowire.

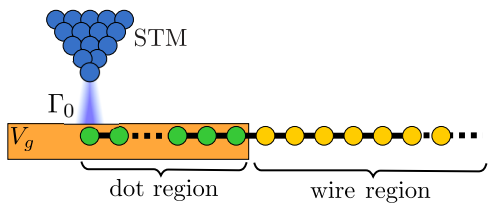

FIG. 2. Schematic idea of the described system. The sites of the quantum dot (green) are side-attached to the superconducting nanowire (yellow) with the proximity-induced electron pairing. Using the STM tip (blue) we can measure the LDOS at each site of the system. Parameter Γ_0 denotes the coupling strength between the STM tip and the probed atom.

Hamiltonian $\mathcal{H}$ of the entire chain can be diagonalized by the Bogoliubov-Valatin transformation [38],

$$c_{i\sigma} = \sum_n (u_{{\rm in}\sigma}\gamma_n - \sigma v^*_{{\rm in}\sigma}\gamma^\dagger_n), \tag{5}$$

where $\gamma_n, \gamma^\dagger_n$ are the quasiparticle fermionic operators and $u_{{\rm in}\sigma}$ and $v_{{\rm in}\sigma}$ are the Bogoliubov–de Gennes (BdG) eigenvectors, respectively. Such unitary transformation implies

$$\mathcal{E}_n\begin{pmatrix} u_{{\rm in}\uparrow}\\ v_{{\rm in}\downarrow}\\ u_{{\rm in}\downarrow}\\ v_{{\rm in}\uparrow}\end{pmatrix} = \sum_j \begin{pmatrix} H_{ij\uparrow} & D_{ij} & S^{\uparrow\downarrow}_{ij} & 0\\ D^*_{ij} & -H^*_{ij\downarrow} & 0 & S^{\downarrow\uparrow}_{ij}\\ S^{\downarrow\uparrow}_{ij} & 0 & H_{ij\downarrow} & D_{ij}\\ 0 & S^{\uparrow\downarrow}_{ij} & D^*_{ij} & -H^*_{ij\uparrow}\end{pmatrix}\begin{pmatrix} u_{{\rm jn}\uparrow}\\ v_{{\rm jn}\downarrow}\\ u_{{\rm jn}\downarrow}\\ v_{{\rm jn}\uparrow}\end{pmatrix}, \tag{6}$$

where $H_{ij\sigma} = -t\delta_{\langle i,j\rangle} - (\mu + \sigma h - V_G\delta_{i\in{\rm dot}})\delta_{ij}$ is the single-particle term, $D_{ij} = \Delta\delta_{ij}$ refers to the induced on-site pairing, and the SOC term (mixing the particles with different spins) is given by $S^{\sigma\sigma'}_{ij} = -i\lambda(\sigma_y)_{\sigma\sigma'}\delta_{\langle i,j\rangle}$, where $S^{\downarrow\uparrow}_{ij} = (S^{\uparrow\downarrow}_{ji})^*$.

To study our system, we will use the local density of states (LDOS) defined as $\rho_i(\omega) = -\frac{1}{\pi}\sum_\sigma {\rm Im}\langle\langle c_{i\sigma}|c^\dagger_{i\sigma}\rangle\rangle$. From numerical solution of the BdG equations (6) we obtain the Green's function $\langle\langle c_{i\sigma}|c^\dagger_{i\sigma}\rangle\rangle$, which formally gives

$$\rho_i(\omega) = \sum_{n\sigma}[|u_{{\rm in}\sigma}|^2\delta(\omega-\mathcal{E}_n) + |v_{{\rm in}\sigma}|^2\delta(\omega+\mathcal{E}_n)]. \tag{7}$$

These physical quantities can be measured experimentally in a relatively simply way [39,40]. In practice this spatially and energy-dependent spectrum can be also probed by a differential conductance $G_i(V) = dI_i(V)/dV$ of the tunneling current $I_i(V)$, which depends on the coupling between the ith atom of the wire and the STM tip [41] (indicated by Γ_0 in Fig. 2).

We have solved the BdG equations (6) for a chain with $N = 200$ sites, choosing $\Delta/t = 0.2$, $\lambda/t = 0.15$, $\mu/t = -2$. For numerical purposes we have also replaced the Dirac delta functions appearing in Eq. (7) by a Lorentzian $\delta(\omega) = \zeta/[\pi(\omega^2+\zeta^2)]$ with a small broadening $\zeta = 0.0025t$.

III. BASIC PROPERTIES

In this section, we will briefly describe basic physical properties of the nanowire without coupled QD. We will also define terminology which will be used in later sections of manuscript.

As we mentioned in Sec. I, in a case of wires with SOC and superconductivity induced by the proximity effect, for some magnetic field h_c phase transition from trivial to nontrivial topological phase occurs. In a case of a one-dimensional chain described by the Hamiltonian $\mathcal{H}$ defined in Sec. II we have $h_c = \sqrt{\Delta^2 + (2t \pm \mu)^2}$ [30,31]. For chosen parameters we have $h_c/t = 0.2$.

Change in magnetic field h leads to the typical evolution of the total density of states (DOS) for this case. Numerical calculation for chosen parameters is shown in Fig. 3. In consequence, due to the finite size effect, we can observe a

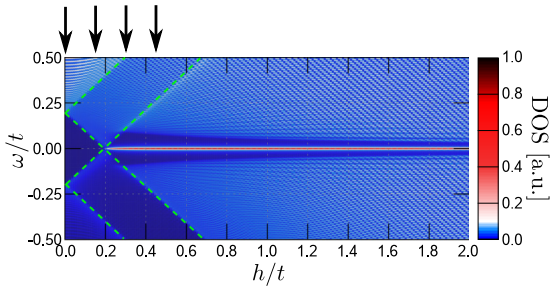

FIG. 3. Total DOS for chain in magnetic field. Result for $k_BT = 0t$, $\mu = -2t$, $\lambda = 0.15t$, and $\Delta = 0.2t$ with $V_g = 0t$. Black arrows represent specific values of h, indicated for further analysis. Green lines specify the regions of the Zeeman shifted induced superconducting gap by proximity effect.

separate line in the DOS. This line corresponds to a singular state of wire [29]. Characteristic structure of the DOS restricted by the asymptotic line (shown by the dashed green line) will be explained below. As we can see, when magnetic field crosses the critical value h_c, the previously closed superconducting gap is reopened partly as a *topological gap* [42].

Now we will introduce previously mentioned terminology, by referring to Fig. 4(a), which schematically shows a change of the DOS by magnetic field h. In the described system, the superconducting gap Δ in wire experimentally corresponds to the *hard gap* induced by proximity effects [21–23], whose value depends on the coupling between the semiconductor wire with the superconducting shell or base [43]. In consequence

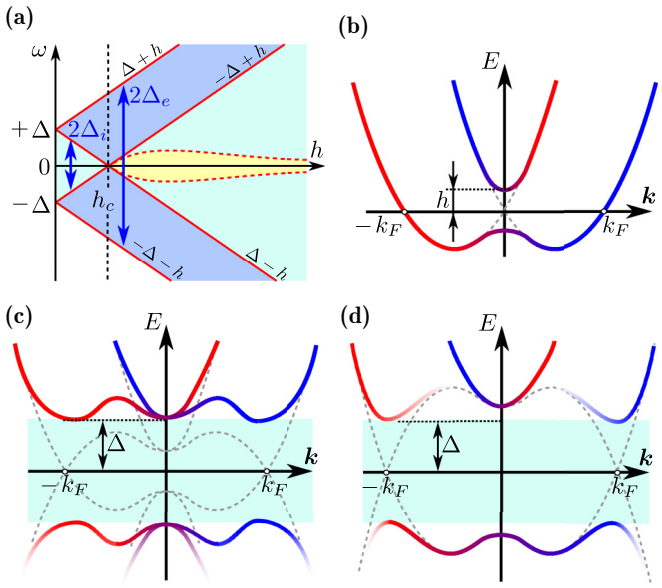

FIG. 4. (a) Schematic representation of the shifted superconducting gaps by magnetic field h, where $2\Delta_e$ and $2\Delta_i$ denote *exterior* and *interior* gaps, respectively. Region for magnetic fields smaller (bigger) than h_c describes the trivial (nontrivial) topological phase. (b)–(d) Band structure obtained in presence of the magnetic field without (b) and with (c,d) superconductivity In the case of trivial (c) and nontrivial (d) topological phases, where the green region 2Δ represents the superconducting gap. Gray dashed line represents band structure in absence of the magnetic field (b) and superconductivity (c,d).

of this, for $h = 0$ we observe a 2Δ gap in the DOS. Increasing h leads to energy levels $\omega = \pm\Delta$ shift (red lines). In this situation, similar to Ref. [42], we can define *exterior gap* $2\Delta_e = 2(\Delta + h)$ and *interior gap* $2\Delta_i = 2(\Delta - h)$ as an energy spacing between external and internal asymptotic line, respectively (blue double-arrows). For $0 < h < h_c$ the *interior* gap decreases, creating *soft gap* with value smaller than *hard gap*. Finally, *interior* superconducting gap is closed in h_c, while for $h > h_c$ *topological gap* reopens (yellow region between dashed red lines). Note that increasing the SOC leads to increased *topological gap* [5].

Experimentally observed *hard gap* depends on magnetic field [12], which is approximately described by the BCS-like relation $\Delta(h) \simeq \Delta\sqrt{1-(h/h_{c2})^2}$ [44], where h_{c2} denotes upper critical magnetic field of superconductor (magnetic field in which *hard gap* will be closed). This dependence effectively leads to experimentally observed suppression of in-gap bound states. However, we assume constant value of Δ, which does not change interpretation of the presented results.

Phase transition from trivial to nontrivial phase, characterized by $\mathbb{Z}_2$ topological invariant [45–47], can be described in relation to band structure of infinite wire with periodic boundary conditions [Figs. 4(b)–4(d)] [12,42,48,49]. In the absence of the superconducting gap, the external magnetic field h leads to the gap opening and lifts spin degeneracy at momentum $k = 0$ [Fig. 4(b)]. Induction of the superconductivity in the wire opens additional gap around the Fermi level $E = 0$ (horizontal axis). The relation between Δ and h, corresponding to the gap opening due to superconductivity and magnetic field, respectively, defines the topologically trivial [Fig. 4(c)] and nontrivial [Fig. 4(d)] regimes. In the trivial topological phase $h < h_c$ [Fig. 4(c)], a new gap at the Fermi momentum $\pm k_F$ emerges and also increases gap at the $k = 0$ because $\Delta > h$ (in accord with "positive" value of the *interior gap* $2\Delta_i$). The situation looks differently in a nontrivial topological phase regime $h > h_c$ [Fig. 4(d)], when $\Delta < h$ (what corresponds to a "negative" value of $2\Delta_i$). In this situation, opening of the superconducting gap at $\pm k_F$ does not change the character of the gap at $k = 0$. Moreover, from a formal point of view, in our system a nontrivial *p-wave* pairing between quasiparticles from this same band is induced. This possibility has been described before [30,31,50–54].

However, in the absence of the boundary conditions (finite wire), discussion of the band structure is unreasonable because momentum is not a good quantum number. Moreover, energy of *bound states* occurring at the *boundaries* of the wire, has symmetrical shape with respect to Fermi energy $\omega = 0$. Nonzero magnetic field applied in the system leads to emergence of ABS in-gap states (with energies $\Delta > |\omega| > \Delta - h$) and ABS with lowest energy defines the boundary of the *interior gap*. Increasing h to a value above h_c allows the MBS to form from the two lowest energy ABSs. Simultaneously, when the lowest energy ABSs merged into MBS, the *topological gap* is created between the new lowest energy ABSs.

In the nontrivial topological phase ($h > h_c$) the zero-energy MBS can be experimentally observed, i.e., in the form of zero-bias peaks in the tunneling conductance measurement [36,40,55,56]. In this type of experiment, the MBS is observed in the form of the zero-bias conductance peak $G_0 = 2e^2/h$ at zero temperature. However, in the finite temperature regime

conductance is significantly reduced, which has been observed experimentally [18] and discussed theoretically [44,56–59]. Therefore, local density of states presented here is a good indicator for the differential conductance [37], however, it strongly depends on temperature and coupling between tip and nanowire [18,49,58–62].

Moreover, the MBS are physically localized at the end of the wire. Length of the wire plays an important role in the realization of MBS wave-function oscillation in space, which is connected to the MBS nonlocality [63]. When considering a sufficiently short wire, overlapping of the two Majorana wave functions is too extensive and the "true" zero-energy MBS cannot be realized, as the MBS annihilate [64–66]. This system requires a meticulously made nanowire [67], because any disorder has a destructive role on the topological phase [47,68–71]. However, local impurity can lead to MBS separation into the pair of new MBS at the *newly* created boundaries of the homogeneous system in topological states [66,72–75].

As we mentioned in Sec. I, the ABSs can be experimentally controlled. Moreover, for some experimental parameter the ABS can coalesce [24] into a *zero-energy bound state* (ZEBS). This feature is realized only in the nontrivial topological phase ($h < h_c$). Because the ZEBS and MBS are zero-energy states, we must mention the differences between those two similar kinds of bound states. First, magnetic field in which ZEBS ($h < h_c$) coalesce is smaller than the one required for MBS to emerge ($h > h_c$). Second, what is more important from a practical point of view, ZEBS do not obey the non-Abelian statistics which is a consequence of different parity with respect to MBS [9,70].

IV. SINGLE QUANTUM DOT

Let us now inspect the superconducting wire comprising $N = 200$ sites with one additional site, representing the normal QD. Evolution of this QD spectrum with respect to the gate voltage V_g is illustrated in Fig. 5 for several magnetic fields h. In the absence of the magnetic field [Fig. 5(a)] and for $V_g/t \leqslant -1.8$ the QD quasiparticles show up in LDOS as the characteristic *devil's staircase* [red ellipse in Fig. 5(a)]. This avoided crossing structure occurs as a consequence of hybridization of the QD energy level with a finite number of the nanowire energy levels. In the regime $V_g/t \in (-1.8, 0.8)$ there appear two ABSs inside the *hard gap*, which never cross each other (as is indicated by the pink double-arrow).

For the $h < h_c$ in the trivial topological phase [Fig. 5(b)], we observe the Zeeman splitting of the initially single spin-degenerate QD levels [white arrows in Fig. 5(b)]. In consequence, the majority spin character for both levels has been disjointed (character of "left" and "right" levels corresponds to majority spin $\downarrow$ and $\uparrow$ quasiparticles, respectively). Moreover, when magnetic field is strong enough, the ABS can cross each other creating ZEBS at two different values of V_g, depending on h (indicated by the green arrows). Characteristic spin-split structure has been also observed [21,76–79].

For strong magnetic field $h > h_c$, at the nontrivial topological phase [Figs. 5(c) and 5(d)], the MBS emerge in the nanowire. Let us remark that such Majorana quasiparticles, for some range of parameters, coexist with the conventional ABS inside the *topological gap*, whose spectral weights depend

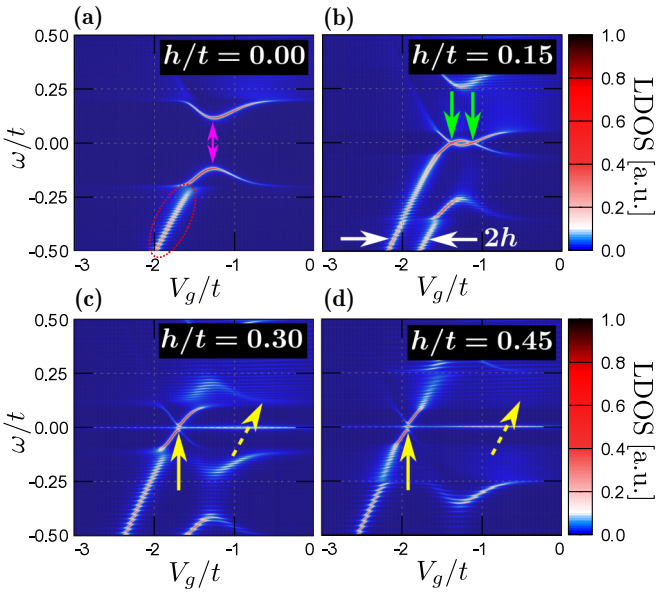

FIG. 5. Evolution of the quantum-dot spectral function with respect to V_g for several magnetic fields, indicated by the black arrows in Fig. 3. Results are obtained for $k_BT = 0t$, $\mu = -2t$, $\lambda = 0.15t$, $\Delta = 0.2t$. Red ellipse in (a) indicates the *devil's staircase* structure.

on h and V_g. Modification of the QD energy level with dominant σ-spin character by V_g leads to two different kinds of resonance with MBS. In the case of the $\uparrow$-like state (in the region indicated by the yellow dashed arrow) *leak* of the MBS into the QD has been observed, whereas for the $\downarrow$-like state there is only a relatively weak resonance (yellow arrows).

It should be mentioned that the possible crossing of the ABS in the absence of the magnetic field is possible when ratio coupling between the QD and nanowire would induce a *hard gap* (in our case t/Δ) that is smaller than one [78]. This scenario can be also realized at the quantum phase transition in the correlated quantum dot [63,78–80] but such an issue is beyond the scope of the present study. For parameters chosen in our system we have $t/\Delta \gg 1$ and the gap between two ABSs inside the *hard gap* could not observed (Fig. 6). In the case studied here, the minimum of the gap mentioned above occurs at $V_g \sim -1.3t$, whereas its extreme value 2Δ is reached either

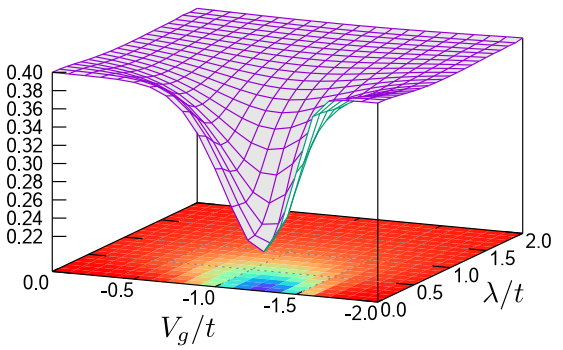

FIG. 6. Effective gap between the ABS (inside the *hard gap*) versus the spin-orbit coupling λ and the gate potential V_g. Results are obtained for the single quantum dot at zero temperature for $\mu = -2t$, $\Delta = 0.2t$, and $h = 0$.

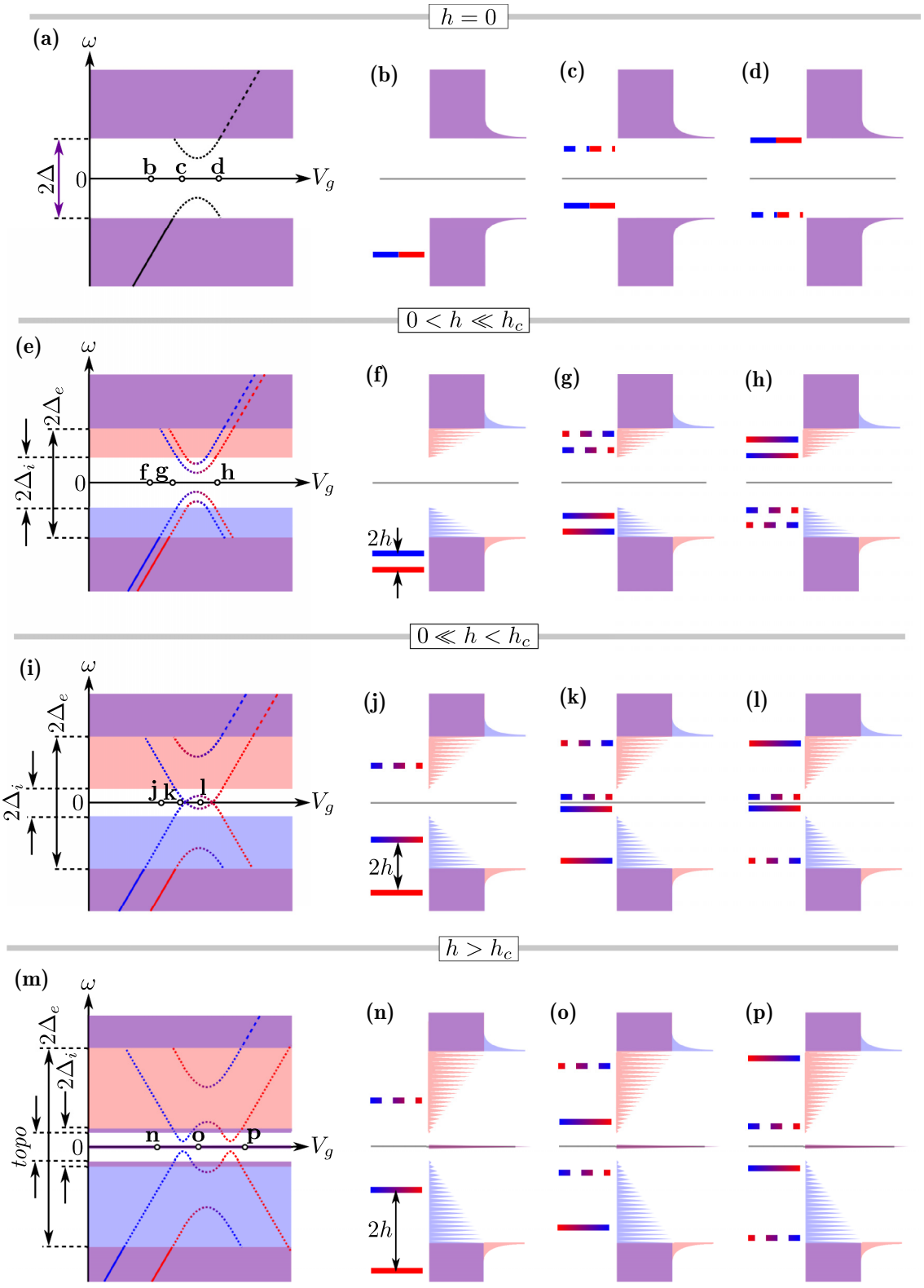

FIG. 7. Schematic representation of the resonance of the dot energy levels and the nanowire with increasing magnetic field (from top to bottom). For every case in the most-left column, solid, dashed, and dotted lines represent occupied, unoccupied, and Andreev bound states, respectively. Moreover, the gray dashed axis line shows the Fermi level and letters on those axes in the most-left column denote the specific gate potential V_g on the quantum dot. In the rest of the columns a solid (dashed) line indicates quasiparticles with dominant particle (hole) character. Colors (red/blue/violet) illustrate the dominant spin ($\uparrow/\downarrow$/degenerate case) of energetic levels. ABSs (f)–(h), (j)–(l), and (n)–(p) inside the external gap become a *mixture* of spins, due to the spin-orbit coupling, hence the transition in colors representing energy levels. Labels 2Δ, $2\Delta_i$, $2\Delta_e$, and *topo* represent the *hard gap*, *interior gap*, *exterior gap*, and *topological gap*, respectively, which have been introduced in Sec. III.

away when gate potential is insignificant or for the strong SOC λ. As we can see in Fig. 5, the ABS crossing can be achieved for some fixed gate potential V_g, in the presence of the magnetic field h which is equal to one-half of the gap between the ABS when magnetic field is absent.

A. Resonance of the quantum-dot levels with Majorana bound states

Let us now explain in detail the asymmetry in the resonance of the QD energy levels with nonowire energy levels, presented previously in Fig. 5. We will do this using the schematic representation of the QD energy levels and nanowire total DOS shown in Fig. 7 and terminology introduced in Sec. III. In the absence of magnetic field [Figs. 7(a)–7(d)], manipulation of gate voltage V_g changes the spin degenerate dot energetic levels with respect to the Fermi level ($\omega = 0$). When states are localized below the superconducting *hard* gap [Fig. 7(b)] we can observe the *devil's staircase* structure. This structure is formed as a consequence of coupling between the QD and nanowire energetic levels–spin conserved (t) and spin-flip (λ) hoppings. ABSs emerge when the QD energy levels are near or inside the *hard gap* [Figs. 7(c) and 7(d)]. The spectral weight of the ABS is leaking from the occupied to the nonoccupied (c → d) levels, converting its character [i.e., see also Fig. 5(a)]. Initially, the negative energy ABS is particle dominated, whereas the positive energy one is hole dominated [Fig. 7(c)]. As the change in V_g progresses, occupation of states is inverted [Fig. 7(d)]. For any nonzero magnetic field h [Figs. 7(e)–7(p)] spin degeneracy is lifted by the Zeeman shift. When $0 < h < h_c$, sharp structures of the ABS are observed in the *hard gap*, creating the *soft gap* which is equal to the *interior gap* ($2\Delta_i$) for this value of magnetic field. If the h is sufficiently small [Fig. 7(e)], the ABS does not cross the Fermi level. When both QD energy levels are localized below the *exterior gap* [Fig. 7(f)], then we observe two separate levels with different spin majority character [see Fig. 5(b)]. As we increase V_g, observed mirrored ABS resonances invert its dominant character from particle to hole (g → h). For high enough magnetic field (but still smaller than h_c) [Figs. 7(i)–7(l)] the ABSs start to cross at zero-energy level. In consequence ABSs coalesce into ZEBS at the Fermi level and the *interior gap* narrows [Fig. 7(i)]. For some value of V_g [Fig. 7(j)] only one pair of ABSs exists inside the *exterior gap* while the ↑ dominant spin level of the QD resides below this gap. Before first coalescing of ABSs [Fig. 7(k)] we observe a situation similar to Fig. 7(g). However, for V_g between points of ABS coalescence (l) energy levels invert. In a case of the $h > h_c$ [Figs. 7(m)–7(p)] the *topological gap* opens and the MBS emerge at $\omega = 0$. In this nontrivial topological phase (with $h > \Delta$) the dot-energy level is shifted enough to treat it independently. For V_g at the point [Fig. 7(n)] the QD energy levels with ↑(↓) dominant spin character are located deep below (near) the *topological gap*. In consequence we observe "in-topological-gap" ABS detached from the ↓-spin QD energy level, which suits minority spin in the whole system. Increase of V_g (o → p) leads to a position of the QD energy level with majority ↑(↓)-spin character near (far above) the *topological gap*, respectively. Additionally, dominant spin component reverses during the topological phase transition [81].

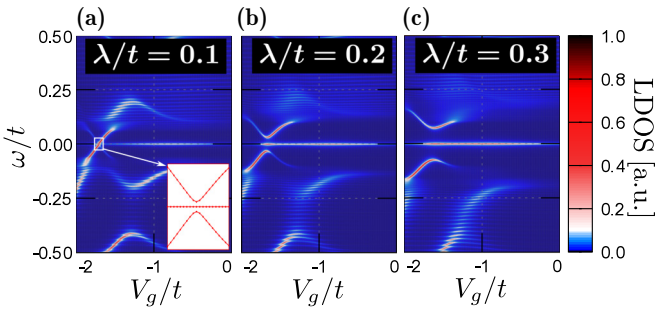

FIG. 8. Effect of the spin-orbit coupling λ on the induced Majorana and Andreev bound states. (a) Inset shows the quasiparticle energies for the zoomed region. Results are obtained for $k_B T = 0t$, $\mu = -2t$, $h = 0.3t$, and $\Delta = 0.2t$.

We must have in mind that quasiparticles with the ↑(↓)-spin character has a dominant (inferior) role in the whole system due to the Zeeman splitting. In this sense MBS at zero-energy level have ↑ spin polarization [9]. Stemming from this, only remaining ↑ dominant spin character energy levels can resonate with the MBS. Following this condition and keeping in mind that the SOC is sufficiently strong in the system, a characteristic structure of avoided crossing occurs, halting the ABS emerged from the inferior ↓-spin QD energy level to cross the zero-energy level. Simultaneously, the ↑-spin dominant QD energy level can resonate with the MBS, which can be clearly seen as an increasing of the spectral weight of the MBS along the dashed arrows in Figs. 5(c) and 5(d).

As a result of the QD coupling to the wire by spin-conserved t and spin-flip λ hopping, the resonance of the QD energy levels with minority ↓-spin character and MBS with ↑ polarization, depends strongly on the spin-orbit coupling. Role of the spin-orbit influence on this behavior is shown Fig. 8, where we compare the resonance of the QD energy levels with the zero-energy MBS for several values of the SOC λ. For any nonzero value of λ, the system supports both the MBS and ABS, coexisting inside the *topological* gap. It can be noticed, that the ABS become gapped [see the inset in Fig. 8(a)] and their avoided crossing behavior becomes significant with an increase of SOC strength λ. At the same time, the MBS gain more and more spectral weight. Furthermore, we also observe constructive influence of the SOC λ on the *devil's staircase* structure, existing outside the *topological* gap. In relation to the previous paragraph, this is a consequence of spin-flip hybridization between QD and wire, supporting the resonance of the ABS and opposite spin character MBS.

B. Different types of zero-energy bound states

We have shown that the ABS can coexist with MBS and sometimes their energies are identical (resonant). Such resonance depends on the quantum-dot energy level, which can by modified by the global Fermi level (i.e., the chemical potential μ), the gate voltage V_g, and the magnetic field h. These quantities affect the ABS and for trivial topological phase ($h < h_c$) lead to emergence of the ZEBS. Here we should remind one that the ZEBS and the MBS are zero-energy states, but emerge in different topological phases (trivial and

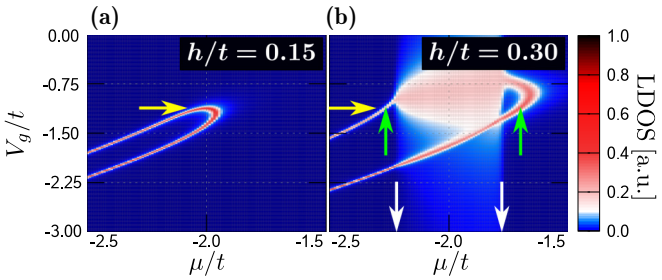

FIG. 9. Modification of the zero-energy LDOS on the quantum-dot site by change μ and V_g in the cases of the phase not supporting (a) and supporting (b) realization of the MBS. Results for $k_BT = 0t$, $\lambda = 0.15t$, and $\Delta = 0.2t$.

nontrivial, respectively). It is illustrated in Fig. 9, where we plot the LDOS of the dot region for $\omega = 0$ versus μ and V_g.

These results refer to the following cases: (i) $h < h_c$, when MBS are not realized for any parameter of the system [Fig. 9(a)]; (ii) $h > h_c$, when for some values of μ, the system can host the MBS [Fig. 9(b); the MBS supporting regime exists between white arrows]. In the first case we can find such regions, where ABSs coalesce into ZEBS [red kink in Fig. 9(a)]. For the latter case, upon varying μ (or h) we can distinguish two regimes: supporting (between white arrows) and nonsupporting (outside white arrows) emergence of the MBS. Inside the first region we can see realization of the (asymmetric) resonance of the QD energy levels with the MBS hosted at the ends of the nanowire. In the second region, similar to previously discussed, we can only see a crossing of the ABS in the ZEBS form. The difference between such resonances has been discussed in previous sections.

The following results are discussed for the cross section of Fig. 9 along $V_g = -1.125t$ indicated by the yellow arrow. Figure 10 shows the LDOS of the QD as a function of the (global) chemical potential μ. We can clearly see that upon varying of μ the coalescing ABS give rise to ZEBS [Fig. 10(a), green arrow]. However, for the nontrivial topological phase [Fig. 10(b)], ZEBS appear only beyond the MBS-supported regime [green arrows outside the region marked by white arrows in Fig. 10(b)]. These results are complementary to Fig. 9(b). Inside this regime there exists the topologically

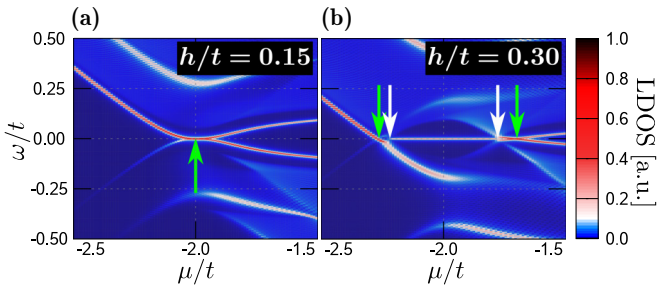

FIG. 10. LDOS on the quantum dot versus the chemical potential μ for the cases not supporting (a) and supporting (b) realization of the MBS. The gate potential is $V_g = -1.125t$ as indicated by the right green arrow in Fig. 5(b). Results are obtained for $k_BT = 0t$, $\lambda = 0.15t$, and $\Delta = 0.2t$.

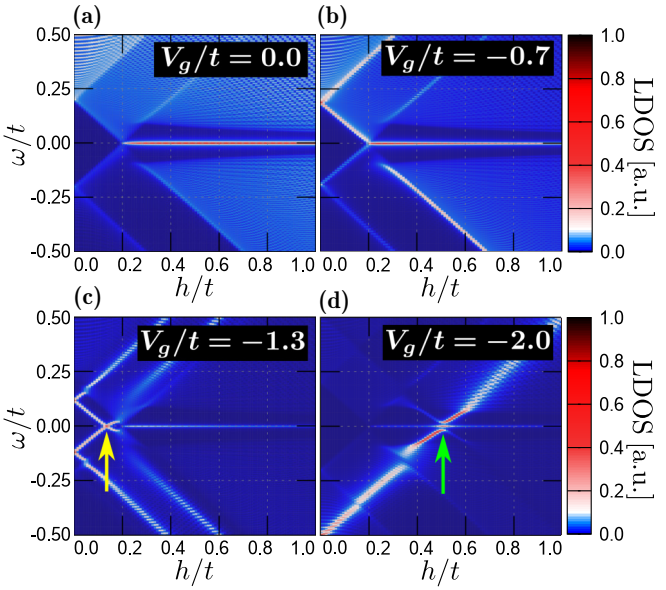

FIG. 11. Evolution of the quantum-dot spectrum with respect to magnetic field h for several gate potentials V_g, as indicated. Results are obtained for $k_BT = 0$, $\mu = -2t$, $\lambda = 0.15t$, and $\Delta = 0.2t$.

protected Majorana states, while for other parameters the ABSs create a new gap around $\omega = 0$.

Further important effects can be seen if we investigate the influence of magnetic field (Fig. 11). As we mentioned previously, h detunes the energy levels of the states with opposite spin character. This is true for the whole studied system. We remind one that, in general, for $h < h_c$ we can observe the ABS or the ZEBS coalesced from ABS, like indicated by yellow arrow in Fig. 11(c), what is in agreement with experimental results [24], whereas the zero-energy MBS can be realized only for $h > h_c$. Similarly to the previous result, increase in h reveals asymmetry in resonance between the QD energy levels with dominant σ-spin character and MBS, what has been explained in Sec. IV A. In some range of gate potential V_g (compare with Fig. 5), with changed h, the dominant $\uparrow$- or $\downarrow$-spin character of the QD energy levels are revealed. In the case of the energy levels with spin majority character ($\uparrow$), resonance between the QD energy level and MBS is favored by spin-conserving hopping [Figs. 11(a) and 11(b)]. For the energy levels with minority character ($\downarrow$), resonance of the QD level and the MBS is more energetically expensive due the fact that the spin-flip hopping λ is smaller than spin-conserved hopping t. As a result, we can observe emergence of the ABS in-topological gap [Fig. 11(d)] and weak resonance with the MBS (green arrow), depending on λ (see Fig. 8). When the QD energy levels penetrate the *hard gap* as the ABS [in weak magnetic field, Fig. 11(c)], the ZEBS is formed (yellow arrow).

V. DOUBLE-SITE QUANTUM DOT

Similar analysis can be performed for the system comprising two additional sites (double-site quantum dot) side-attached to the hybrid nanowire. In this case, we observe two pairs of the ABS appearing in the spectrum of such dots

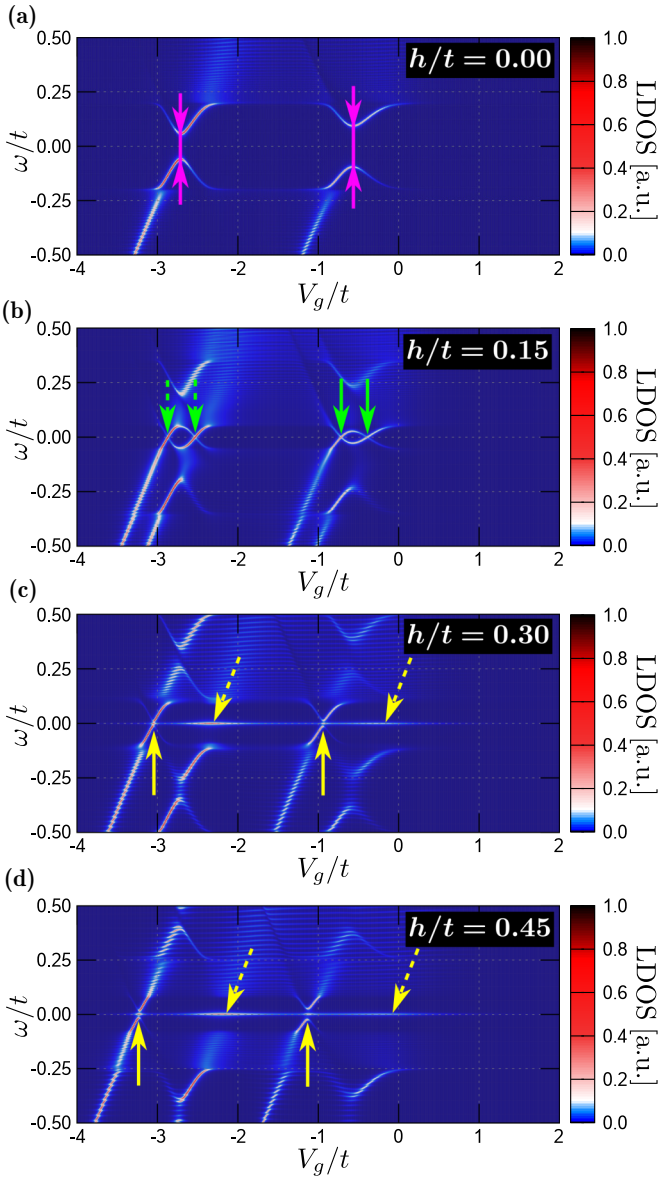

FIG. 12. Evolution of the double quantum-dot LDOS with respect to the gate voltage V_g for several magnetic fields, indicated by the white arrows in Fig. 3. Results are obtained for $k_BT = 0t$, $\mu = -2t$, $\lambda = 0.15t$, and $\Delta = 0.2t$.

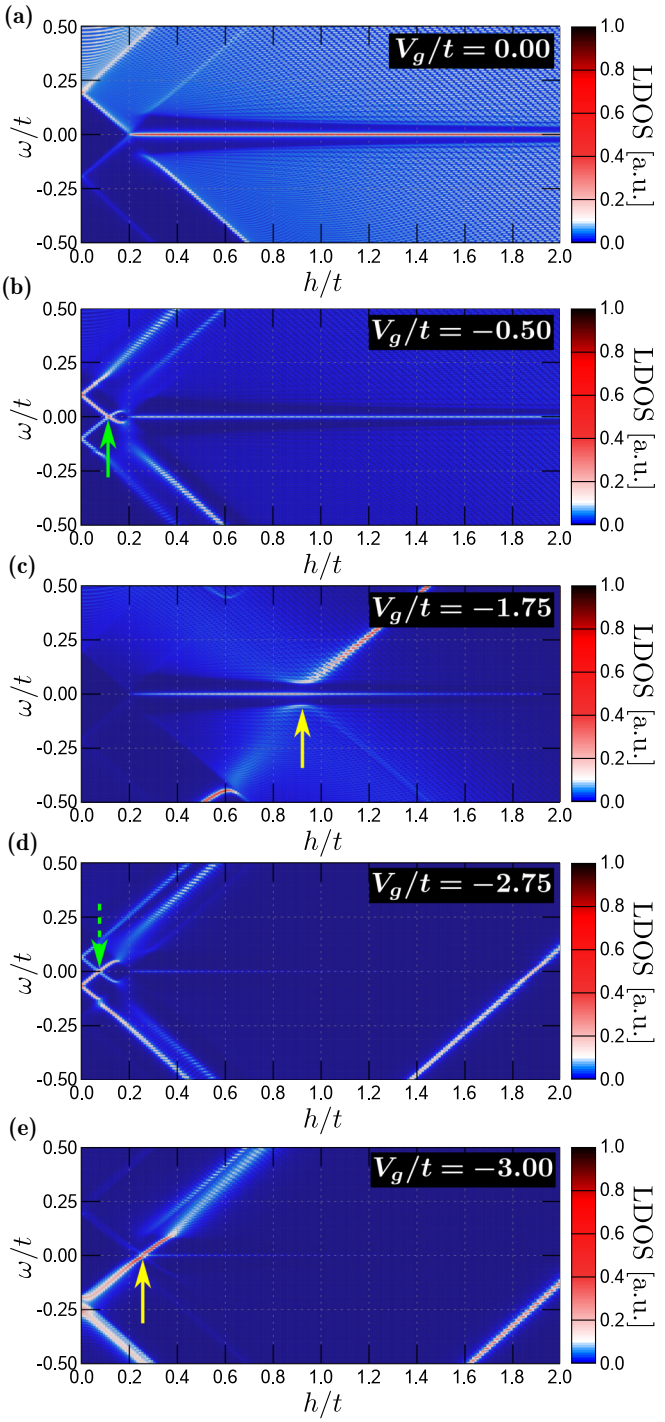

FIG. 13. Influence of the magnetic field h on the LDOS of the double quantum dot for different values of the gate voltage V_g, as indicated. Result are obtained for $k_BT = 0t$, $\mu = -2t$, $\lambda = 0.15t$, and $\Delta = 0.2t$.

(Fig. 12). We notice that for $h = 0$ these pairs of ABSs are split by different energy gaps [indicated by the pink arrows in Fig. 12(a)]. For this reason, within a range of weak magnetic field $h < h_c$ we can observe either one or two pairs of the spin-split ZEBS [marked by the solid and dashed green arrows in Fig. 12(b)]. In the regime of nontrivial topological phase (for $h > h_c$) we see emergence of the zero-energy MBS [yellow solid and dashed arrows in Figs. 12(c) and 12(d)]. When the MBS (with ↑ majority spin character of the system) hosted on the wire, coincides with the minority spin character (↓) double-site QD energy levels [yellow solid arrows in Figs. 12(c) and 12(d)], we can observe its existence in the *topological gap* while ABSs do not cross at zero-energy level. In other words, the ABS separate from the zero-energy Majorana mode as a consequence of weak coupling between QD and the strong one in the wire due to the spin-flip hopping λ. Regarding the case of energy levels with ↑-spin character (dashed yellow arrows), their bound states do not enter the *topological gap* but resonate with the MBS at the zero-energy level. Figure 13 shows the double quantum-dot spectrum as a function of the magnetic field h for several values of the gate voltage V_g. Again, we notice that V_g controls the spectral

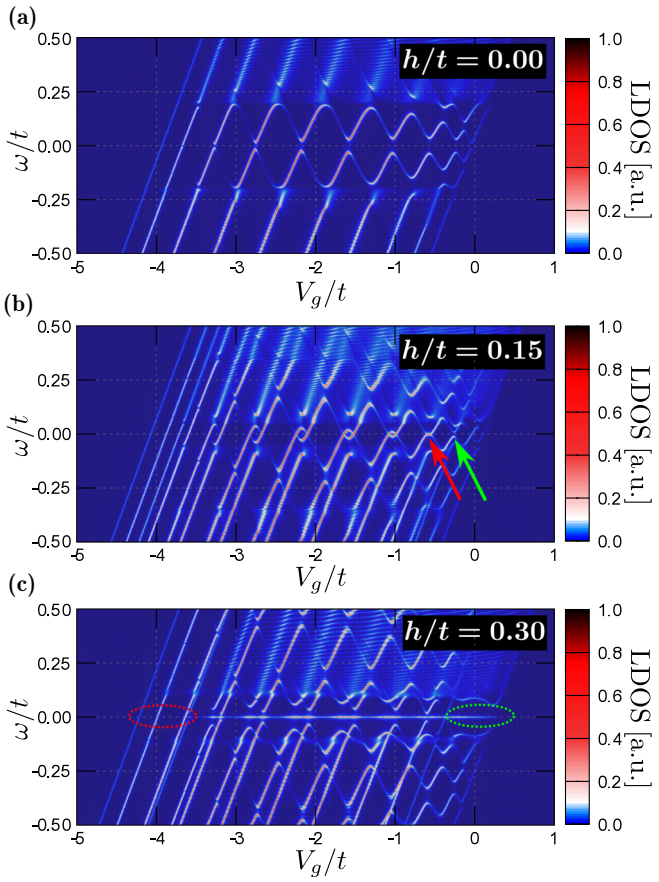

FIG. 14. Gate voltage dependence of the LDOS obtained at zero temperature for the quantum dot comprising 10 sites, using $\mu = -2t$, $\lambda = 0.15t$, and $\Delta = 0.2t$. (c) Red (green) dotted ellipses correspond to the region where only the quantum-dot energy levels with $\downarrow$ ($\uparrow$)-spin character exist.

weight of the Majorana mode leaking into the QD region in the nontrivial topological phase (above the critical magnetic field $h > h_c$).

VI. MULTISITE QUANTUM DOT

In realistic quantum systems the ABS can sometimes originate from a multitude of the energy levels existing in a subgap regime. We shall model such a situation here, considering a piece of the nanowire (sketched in Fig. 2) whose energy levels can be identified as the finite number of lattice sites in this complex structure. Such systems can be realized experimentally, e.g., in the carbon nanotube superconducting device [76]. Similar effects can be relevant to the experiment reported by Deng *et al.* [24]. Another possible realization could refer to the multilevel structure obtained by the modern experimental technique, designing the quantum dot with atomic precision [82]. Due to the proximity effect, we can expect appearance of the N pairs ABS [21,22,24,76], where N is the number of the sites in the QD region. In our calculations for the multilevel dot we shall focus on $N = 10$ sites.

Figure 14 shows variation of the normal nanowire spectrum with respect to the gate voltage V_g for several magnetic fields h, as indicated. For $h = 0$ [Fig. 14(a)] we observe N quasiparticle branches, which become doubled at low energies (due to particle-hole mixing). For the weak magnetic field $h < h_c$ [Fig. 14(b)] we can observe the Zeeman splitting of the initial quasiparticle branches. In a low energy regime these bound states eventually reveal either a crossing (red arrow) or avoided crossing (green arrow), depending on the gate voltage V_g. Finally, when hybrid-nanowire transitions to nontrivial topological phase $h > h_c$, we can observe resonance of the QD energy levels with MBS hosted in the nanowire [Fig. 14(c)], similarly to previous results, but different form for levels with majority or minority spin character.

In consequence of the asymmetric resonances of the QD energy levels with minority and majority spin types, we observe different behaviors of these levels in the subgap region [Fig. 14(c)]. The QD energy levels with the minority spin ($\downarrow$) character are insensitive to the existence of the MBS zero-energy level in the wire (red dotted ellipse), while in the case of majority spin ($\uparrow$) complete resonance is observed (green dotted ellipse). In the case of the intermediate V_g regime (between red and green dotted ellipses), the spectral weight of the MBS weakly oscillates with a varying V_g as a consequence of various interplay between the QD energy levels, depending on their dominant spin component.

From a practical point of view it is important to know what are the spatial profiles of the zero-energy bound states of the nanowire, due to their dependence on the magnetic field. For $h < h_c$ they correspond to crossings of the ZEBS whereas for $h > h_c$ they refer to the MBS, respectively. As mentioned in Sec. III, the zero-energy MBS is characterized as the localized, oscillating in space, wave function formed at the end of the wire. Similarly, the ABS wave functions are localized in the QD region of the studied system. In both cases these zero-energy bound states can leak from the QD to the nanowire region (in the case of the ZEBS) or *vice versa* (when MBS is present), via the hybridization between both parts. Figure 15 presents the spatially dependent spectral weight of the zero-energy ($\omega = 0$) quasiparticles. Let us remark that $i \in \langle 1,10\rangle$ in this case correspond to the multisite QD connected to the hybrid nanowire. For some value of the magnetic field smaller than h_c [Fig. 15(a)], but bigger than the gap between ABS in the absence of the magnetic field, we can observe several crossings of the ABS (visible as red lines). These ZEBS are localized mainly in the QD region and leak into the nanowire region. The situation looks different in a nontrivial topological phase [Fig. 15(b)], where the MBS are present. In consequence, when QD energy levels change (controlled by gate voltage V_g), we can observe a shift of the MBS initially localized in the end of the wire to the dot region.

By inspecting Fig. 15 we can also notice spatial oscillations of the zero-energy quasiparticles, both in the trivial ($h < h_c$) and nontrivial ($h > h_c$) topological phases. This behavior is observable near the edges (spectrum of the entire system is shown in Fig. 16). In the trivial topological phase [Fig. 16(a)] such oscillations appear mainly in the QD and leak partially to the wire (green dotted ellipse). The situation changes completely for the nontrivial superconducting state [Fig. 16(b)], where the MBS oscillations (red arrows) exist on both sides of the interface and leak to the QD region (green dotted ellipse). In the second case the spatial oscillations are very pronounced, as has been mentioned in Sec. III.

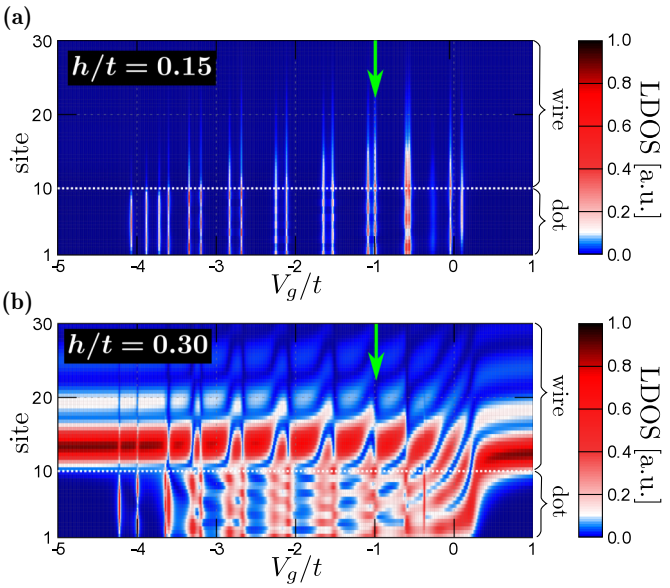

FIG. 15. Spatial profiles of the ABS and/or MBS obtained at $\omega = 0$ for the normal nanowire, comprising 10 sites. (a) The ABS of the trivial superconducting state ($h < h_c$); (b) Illustration of the spatial profiles of the MBS in the topologically nontrivial superconducting state ($h > h_c$). Results are obtained for $k_BT = 0t$, $\mu = -2t$, $\lambda = 0.15t$, and $\Delta = 0.2t$. Dotted white line shows the boundary between the quantum dot and wire regions.

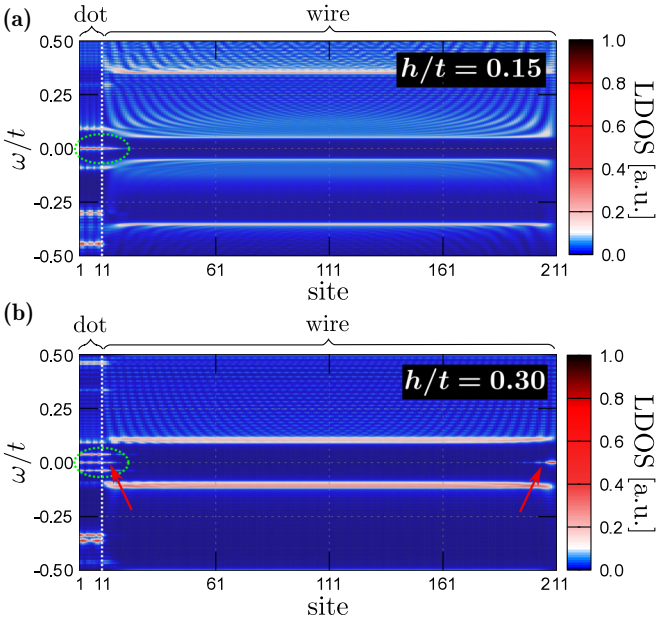

FIG. 16. LDOS along the quantum-dot hybrid nanowire in the cases of the phase not supporting (a) and supporting (b) realization of the MBS. Dot regions are localized below site 11, while the superconducting wire is above site 10. Results for $k_BT = 0t$, $\mu = -2t$, $\lambda = 0.15t$, and $\Delta = 0.2t$. Bias voltages are fixed as $V_g = -0.99$, which corresponds to one of the ABS-resonance levels shown in Fig. 15 as green arrows. The dotted white line shows the boundary between the quantum-dot and wire regions. Red arrows show a pair of MBS.

VII. QUANTUM DEVICE WITH TUNABLE ANDREEV AND MAJORANA BOUND STATES

Finally we propose an experimentally feasible device (sketched in Fig. 17) for controllable realization of various types of the bound states using electrostatic means. Motivation to realization of the device in the proposed form, is provided by the results from previous sections, which suggest multiple possible outcomes: (i) realization and controlling of ZEBS from coalescing ABS (for $h < h_c$); (ii) ZEBS leakage from the QD to the nanowire region (for $h < h_c$); (iii) MBS leakage from the nanowire to the QD region (for $h > h_c$). In analogy to the setup used by Deng *et al.* [24] we suggest using the semiconducting wire whose external parts are epitaxially covered by the superconductors (SC1 and SC2). Such a system resembles the typical SNS junction [83], however, we omit the phase dependence as superconductors SC1 and SC2 can be taken as made from the same material. The central piece (which is not covered by superconductors) is treated as the multilevel QD in which energy levels can be varied by the gate potential V_g (orange region, similar to Fig. 1). Pairs of gates at the ends of the wire (pink), play a crucial role in this setup as they employ the means to measure and verify the existence of zero-bias MBS peaks, e.g., in a differential conductance discussed in Sec. III. The change of the (global) chemical potential μ can be realized by changing the voltage at the base (green). By applying the STM tip to the central QD region, one can probe the different types of bound states in the differential conductance for each individual site. We have in mind that the whole device should be in the external magnetic field, directed along the wire. Moreover, in generality the SC1 and SC2 may be different materials. As a consequence of this, only one part of the nanowire can pass to the nontrivial topological phase, supporting the realization of the MBS, which should be observed as a zero-bias peak in the differential conductance between pairs of the gates, i.e., G1-G1′ and G2-G2′ (or G3-G3′ and G4-G4′). On the other hand, simultaneous measurements carried out by pairs of the gates and the STM can verify the possibility of the bound states leaking from the QD to the nanowire region or *vice versa*.

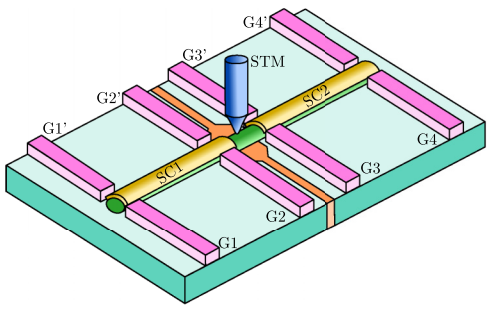

FIG. 17. Sketch of the proposed device for a tunable realization of the Andreev or Majorana bound states. Semiconducting wire (green) is epitaxially covered by two pieces of the superconducting material (SC1 and SC2). The uncovered part of the wire is the multisite quantum dot, for which energy levels are constrained by the underlying gate (pink). The side-attached pairs of gates (i.e., G1-G1′, G2-G2′, etc.) can be used to measure, e.g., differential conductance. Using the STM tip (blue) one can detect the bound states present in the quantum-dot region.

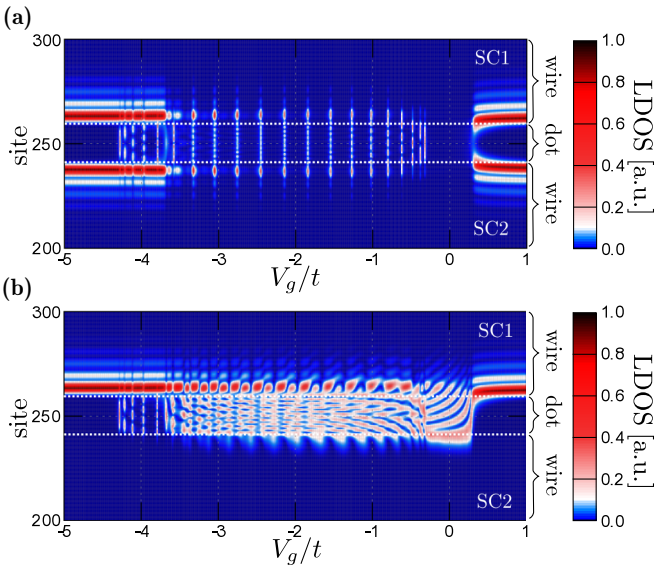

FIG. 18. Spectral weight of the zero-energy quasiparticles induced in the multilevel quantum dot (sites from 240 to 260) coupled the two nanowires (see Fig. 17). Results are obtained for $k_BT = 0t$, $\mu = -2t, \lambda = 0.15t$, and $h = 0.3t$ assuming either $\Delta = 0.2t$ for both superconducting wires (a) or $\Delta = 0.2t$ for the sites $i > 260$ and $\Delta = 0.4t$ for the sites $i < 240$, respectively. The dotted white line shows the boundary between the quantum-dot and wire regions.

The STM-type measurement in the central region of the proposed device, also can be useful for studying or checking the nature of the realized bound states. It has been recently emphasized that the Majorana quasiparticles can be distinguished from the usual Andreev states by the spin-polarized spectroscopy called the selective equal spin Andreev reflections (SESARs) [84] or spin selective Andreev reflection (SSAR) [85,86]. This type of spectroscopy, unambiguously distinguishes between the "true" and "fake" Majorana quasiparticles [87,88], which has been used successfully for, e.g., the detection of a zero-bias peak in the $Bi_2Te_3/NbSe_2$ heterostructure [89,90] or in the case of the magnetic atom chain [17,27,91–93].

Now we will show and discuss numerical results, which should be realized in the device described above. We considered the QD comprising 20 sites ($240 < i < 260$). Figure 18 shows the zero-energy quasiparticle spectrum for two situations: (i) when both nanowires are in the nontrivial topological phase [Fig. 18(a)], and (ii) when one part (SC1) is the nontrivial topological phase, whereas the other one (SC2) is not [Fig. 18(b)]. In both cases the zero-energy QD levels are available for some discrete values of the gate potential V_g, approximately in the voltage regime of $-4.5 \leqslant V_g/t \leqslant -0.5$. What is also important, in both cases, outside this range of V_g we can observe a hosting of the MBS in the SC1 region (and in the SC2 region in the first case). ZEBS available on the QD and MBS hosted in the wires, can be lead to a resonance between them in a controlled fashion. As a consequence we can check features described in previous sections, a difference in resonance of the MBS with the QD energy levels with majority or minority spin character [asymmetry in Fig. 18(a) around V_g equals $-4t$ and $0t$]. Another possibility is an

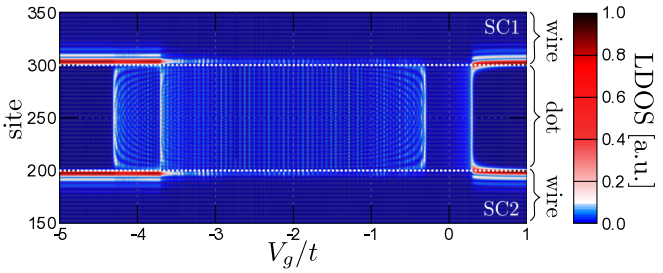

FIG. 19. This same as in Fig. 18(a) but for the broader central quantum-dot region, comprising 100 sites ($200 \leqslant i \leqslant 300$). Dotted white lines show the boundary between the quantum-dot and wire regions.

experimental study of the leaking of the MBS from one part of the device to the second one via the QD region. Moreover, here we have two possibilities: (i) when MBS is hosted in both wires [Fig. 18(a)], this causes an *interference* between two different Majorana quasiparticles [94,95], and (ii) when only one wire hosts the MBS [Fig. 18(b)], this gives the possibility of studying the MBS leakage from the first to the second wire in the ZEBS form [Fig. 18(b)]. A similar suggestion can be found in Ref. [96], where the authors described the expected experimental result of conductance spectroscopy in a nontopological-topological superconductor junction, which is a building block of our proposed device. In both cases, measurement of the differential conductance between pairs of gates (i.e., G1-G1′, etc.) in the described device, can be helpful to verify the realization of the zero-energy-type bound states in the form of the zero-bias peak or the ABS in the case of nonzero bias.

It should be mentioned that our calculation shows an important role of the finite number of available QD energy levels (compare, e.g., Figs. 18(a) and 19). Suggested measurement should be more apparent for QD with a smaller number of energy levels (which in our case corresponds to number of sites in the dot region).

VIII. SUMMARY

Recent experiments suggest the possibility of realization of the zero-energy bound state in a hybrid-nanowire structure (Sec. I), which can be interpreted as a Majorana bound state, with its characteristic features (Sec. III). Motivated by the results obtained by Deng *et al.* [24], who reported the possibility of inducing the bound states in the quantum dot in a controllable way, we described the experimental setup (quantum-dot hybrid nanowire structure), using the microscopic model (Sec. II) and solving it in real space by the Bogoliubov–de Gennes technique.

In Sec. IV we studied properties of the system with the one-site quantum dot adjoined to the nanowire. In particular, we analyzed the following: (i) possible influence of gate voltage V_g on the bound state realized in the quantum dot, and (ii) mutual relation between bound states in the quantum dot and the nanowire region. We showed that the Andreev bound states, observed for some value of the magnetic field inside the *hard* superconducting gap, can coalesce in a controllable way, creating zero-energy bound states. In relation to this, the zero-energy Majorana bound states can be realized only when

magnetic field is sufficiently large. Our results are in agreement with those presented in Ref. [24].

Mutual influence of those two types of bound states is possible as a consequence of shared existence at the zero-energy level. Therefore, it is possible for bound states to leak from the quantum dot to the nanowire region or *vice versa*. Moreover, we showed an asymmetry between resonance of the Majorana bound state and the quantum-dot energy levels. We explained both results as a consequence of (i) change in dominant spin character of quantum-dot energy levels by magnetic field (the majority $\uparrow$ and minority $\downarrow$ spin character), and (ii) different resonance between the Majorana bound states (with $\uparrow$ character) and the quantum-dot energy levels (corresponding to $\uparrow$ and $\downarrow$).

This can also be observed as an influence of the spin-orbit coupling on the relation between the Andreev bound state, which penetrates the *topological gap* and zero-energy Majorana bound states. Increase in the spin-orbit coupling leads to an avoided crossing of the Andreev bound state with a dominant $\downarrow$-spin character and is accompanied by transfer of the spectral weight to the Majorana bound state. This effect is not observed when the quantum-dot energy level has $\uparrow$-spin character.

Those results also can be observed in a more general structure with the multisite quantum dot (e.g., two-site or multisite quantum dot described in Sec. V and Sec. VI, respectively). In this more realistic picture of the quantum dot, we found that the Majorana bound state can resonate with several quantum-dot energy levels with dominant $\uparrow$-spin character, which is visible as a series of the discrete quantum levels in the quasiparticle spectrum. We showed that the Majorana bound states leak from the wire to the quantum-dot region and observed the pronounced quantum oscillations in their spatial profiles. These effects indicate a tendency towards spatial broadening of the Majorana modes.

In Sec. VII we proposed a quantum device in the form of a semiconductor nanowire, whose two parts are covered by the superconductor. The remaining uncovered part can be treated as a quantum dot, with a finite number of available energy levels. This type of device can be used in the realization of described properties, i.e., interplay between different types of bound states. In the regime of the parameter supporting the realization of the Majorana quasiparticles, the presented nanodevice can help to distinguish the differences in resonance between zero-energy bound states with a different dominant spin character. We hope that such a device would be stimulating for further studies of the Majorana quasiparticles and their *interactions* with other kinds of bound states.

Experimental results obtained by Deng *et al.* [24] have been intensively discussed by many groups studying the tunneling conductance [44,57–59]. However, the zero-bias conductance peak does not provide definitive evidence for Majorana zero modes [44]. In relation to this, the zero mode occurring as a consequence of the usual Andreev bound state (in a trivial topological phase) is generally expected to produce a zero-bias conductance peak of height varying between 0 to $4e^2/h$. We must have in mind, however, influence of additional physical effects (e.g., finite temperature [58]) leading to reduction of the conductance value, as mentioned in Sec. III. This type of behavior is important in distinguishing the zero-energy feature related to the "trivial" Andreev from the "nontrivial" Majorana bound states [44].

To this end, let us highlight the main findings of our paper. Interplay between the quantum-dot and nanowire energy levels strongly depend on the *topological state* of the system (cf. Fig. 9). In the case of the trivial topological phase, the dot energy level creates zero-energy bound states via Andreev bound states only for some specific values of the gate potential and magnetic field. Contrary to this, in the nontrivial topological phase the Majorana zero-energy bound states can be observed in a wide range of parameters. We also inspected *leakage* of the Majorana bound states from the nanowire to quantum-dot region. In relation to the previous work addressing interplay between the quantum-dot energy levels with a nonlocality of the Majorana zero modes [63], we discussed influence of the coupling in spin-conserved and in spin-flip channels between the quantum dot and the nanowire. We showed that this process strongly depends on the dominant spin component of the quantum-dot energy states. Similar behavior has been discussed in the context of spin-dependent coupling between the quantum dot and the nanowire [97]. Moreover, we have proposed an experimentally feasible device for studying such a *leakage* effect and detecting the Majorana quasiparticles. This device can be helpful in experimental verification of the described behavior and in practical realization of the true Majorana qubits [98]. Realizations of this proposed device could be well controlled electrostatically, in which the Majorana bound states could emerge or disappear in the quantum-dot region. Similarities have been previously suggested for quantum computing based on the Majorana quasiparticles [99].

Note added. During the reviewing process of this article, we became aware of Ref. [100], describing detection of the topological phase transition in nanowires using the quantum dot analogous to the properties described by us in Sec. IV.

ACKNOWLEDGMENTS

We kindly thank Sz. Głodzik, J. Klinovaja, M. P. Nowak, M. M. Maśka, J. Tworzydło, and D. P. Wójcik for careful reading of the manuscript, valuable comments, and discussions. We also thank M. T. Deng for consultation and remarks on Sec. VII. This work was supported by the National Science Centre (NCN, Poland) under Grants No. UMO-2016/20/S/ST3/00274 (A.P.) and No. DEC-2014/13/B/ST3/04451 (A.K. and T.D.).

[1] N. Read and D. Green, Paired states of fermions in two dimensions with breaking of parity and time-reversal symmetries and the fractional quantum Hall effect, Phys. Rev. B **61**, 10267 (2000).

[2] A. Y. Kitaev, Unpaired Majorana fermions in quantum wires, Phys.-Usp. **44**, 131 (2001).

[3] L. Fu and C. L. Kane, Superconducting Proximity Effect and Majorana Fermions at the Surface of a Topological Insulator, Phys. Rev. Lett. **100**, 096407 (2008).

[4] Ch. Nayak, S. H. Simon, A. Stern, M. Freedman, and S. Das Sarma, Non-Abelian anyons and topological quantum computation, Rev. Mod. Phys. **80**, 1083 (2008).

[5] J. D. Sau, S. Tewari, R. M. Lutchyn, T. D. Stanescu, and S. Das Sarma, Non-Abelian quantum order in spin-orbit-coupled semiconductors: Search for topological Majorana particles in solid-state systems, Phys. Rev. B **82**, 214509 (2010).

[6] J. Alicea, Y. Oreg, G. Refael, F. von Oppen, and M. P. A. Fisher, Non-Abelian statistics and topological quantum information processing in 1D wire networks, Nat. Phys. **7**, 412 (2011).

[7] D. Rainis and D. Loss, Majorana qubit decoherence by quasiparticle poisoning, Phys. Rev. B **85**, 174533 (2012).

[8] B. van Heck, A. R. Akhmerov, F. Hassler, M. Burrello, and C. W. J. Beenakker, Coulomb-assisted braiding of Majorana fermions in a Josephson junction array, New J. Phys. **14**, 035019 (2012).

[9] D. Sticlet, C. Bena, and P. Simon, Spin and Majorana Polarization in Topological Superconducting Wires, Phys. Rev. Lett. **108**, 096802 (2012).

[10] D. Aasen, M. Hell, R. V. Mishmash, A. Higginbotham, J. Danon, M. Leijnse, T. S. Jespersen, J. A. Folk, Ch. M. Marcus, K. Flensberg, and J. Alicea, Milestones Toward Majorana-Based Quantum Computing, Phys. Rev. X **6**, 031016 (2016).

[11] V. Mourik, K. Zuo, S. M. Frolov, S. R. Plissard, E. P. A. M. Bakkers, and L. P. Kouwenhoven, Signatures of Majorana fermions in hybrid superconductor-semiconductor nanowire devices, Science **336**, 1003 (2012).

[12] A. Das, Y. Ronen, Y. Most, Y. Oreg, M. Heiblum, and H. Shtrikman, Zero-bias peaks and splitting in an Al-InAs nanowire topological superconductor as a signature of Majorana fermions, Nat. Phys. **8**, 887 (2012).

[13] M. T. Deng, C. L. Yu, G. Y. Huang, M. Larsson, P. Caroff, and H. Q. Xu, Anomalous zero-bias conductance peak in a Nb-InSb nanowire-Nb hybrid device, Nano Lett. **12**, 6414 (2012).

[14] L. P. Rokhinson, X. Liu, and J. K. Furdyna, The fractional a.c. Josephson effect in a semiconductor-superconductor nanowire as a signature of Majorana particles, Nat. Phys. **8**, 795 (2012).

[15] H. O. H. Churchill, V. Fatemi, K. Grove-Rasmussen, M. T. Deng, P. Caroff, H. Q. Xu, and C. M. Marcus, Superconductor-nanowire devices from tunneling to the multichannel regime: Zero-bias oscillations and magnetoconductance crossover, Phys. Rev. B **87**, 241401 (2013).

[16] A. D. K. Finck, D. J. Van Harlingen, P. K. Mohseni, K. Jung, and X. Li, Anomalous Modulation of a Zero-Bias Peak in a Hybrid Nanowire-Superconductor Device, Phys. Rev. Lett. **110**, 126406 (2013).

[17] B. E. Feldman, M. T. Randeria, J. Li, S. Jeon, Y. Xie, Z. Wang, I. K. Drozdov, B. Andrei Bernevig, and A. Yazdani, High-resolution studies of the Majorana atomic chain platform, Nat. Phys. **13**, 286 (2017).

[18] F. Nichele, A. C. C. Drachmann, A. M. Whiticar, E. C. T. O'Farrell, H. J. Suominen, A. Fornieri, T. Wang, G. C. Gardner, C. Thomas, A. T. Hatke, P. Krogstrup, M. J. Manfra, K. Flensberg, and Ch. M. Marcus, Scaling of Majorana Zero-Bias Conductance Peaks, Phys. Rev. Lett. **119**, 136803 (2017).

[19] S. Nadj-Perge, I. K. Drozdov, J. Li, H. Chen, S. Jeon, J. Seo, A. H. MacDonald, B. A. Bernevig, and A. Yazdani, Observation of Majorana fermions in ferromagnetic atomic chains on a superconductor, Science **346**, 602 (2014).

[20] P. Krogstrup, N. L. B. Ziino, W. Chang, S. M. Albrecht, M. H. Madsen, E. Johnson, J. Nygård, C. M. Marcus, and T. S. Jespersen, Epitaxy of semiconductor–superconductor nanowires, Nat. Mater. **14**, 400 (2015).

[21] W. Chang, M. S. Albrecht, S. T. Jespersen, F. Kuemmeth, P. Krogstrup, J. Nygård, and M. C. Marcus, Hard gap in epitaxial semiconductor–superconductor nanowires, Nat. Nanotech. **10**, 232 (2015).

[22] S. M. Albrecht, A. P. Higginbotham, M. Madsen, F. Kuemmeth, T. S. Jespersen, J. Nygård, P. Krogstrup, and C. M. Marcus, Exponential protection of zero modes in Majorana islands, Nature (London) **531**, 206 (2016).

[23] Ö. Gül, H. Zhang, F. K. de Vries, J. van Veen, K. Zuo, V. Mourik, S. Conesa-Boj, M. P. Nowak, D. J. van Woerkom, M. Quintero-Pérez, M. C. Cassidy, A. Geresdi, S. Koelling, D. Car, S. R. Plissard, E. P. A. M. Bakkers, and L. P. Kouwenhoven, Hard superconducting gap in InSb nanowires, Nano Lett. **17**, 2690 (2017).

[24] M. T. Deng, S. Vaitiekenas, E. B. Hansen, J. Danon, M. Leijnse, K. Flensberg, J. Nygård, P. Krogstrup, and C. M. Marcus, Majorana bound state in a coupled quantum-dot hybrid-nanowire system, Science **354**, 1557 (2016).

[25] A. Yazdani, B. A. Jones, C. P. Lutz, M. F. Crommie, and D. M. Eigler, Probing the local effects of magnetic impurities on superconductivity, Science **275**, 1767 (1997).

[26] R. Pawlak, M. Kisiel, J. Klinovaja, T. Meier, S. Kawai, T. Glatzel, D. Loss, and E. Meyer, Probing atomic structure and Majorana wavefunctions in mono-atomic Fe chains on superconducting Pb surface, npj Quantum Inf. **2**, 16035 (2016).

[27] M. Ruby, B. W. Heinrich, Y. Peng, F. von Oppen, and K. J. Franke, Exploring a proximity-coupled Co chain on Pb(110) as a possible Majorana platform, Nano Lett. **17**, 4473 (2017).

[28] D. Chevallier, D. Sticlet, P. Simon, and C. Bena, Mutation of Andreev into Majorana bound states in long superconductor-normal and superconductor-normal-superconductor junctions, Phys. Rev. B **85**, 235307 (2012).

[29] D. Chevallier, P. Simon, and C. Bena, From Andreev bound states to Majorana fermions in topological wires on superconducting substrates: A story of mutation, Phys. Rev. B **88**, 165401 (2013).

[30] M. Sato and S. Fujimoto, Topological phases of noncentrosymmetric superconductors: Edge states, Majorana fermions, and non-Abelian statistics, Phys. Rev. B **79**, 094504 (2009).

[31] M. Sato, Y. Takahashi, and S. Fujimoto, Non-Abelian topological orders and Majorana fermions in spin-singlet superconductors, Phys. Rev. B **82**, 134521 (2010).

[32] J. Chen, P. Yu, J. Stenger, M. Hocevar, D. Car, S. R. Plissard, E. P. A. M. Bakkers, T. D. Stanescu, and S. M. Frolov, Experimental phase diagram of zero-bias conductance peaks in superconductor/semiconductor nanowire devices, Sci. Adv. **3**, e1701476 (2017).

[33] S. Gazibegovic, D. Car, H. Zhang, S. C. Balk, J. A. Logan, M. W. A. de Moor, M. C. Cassidy, R. Schmits, D. Xu, G. Wang, P. Krogstrup, R. L. M. Op het Veld, K. Zuo, Y. Vos, J. Shen, D. Bouman, B. Shojaei, D. Pennachio, J. S. Lee, P. J. van Veldhoven, S. Koelling, M. A. Verheijen, L. P. Kouwenhoven, Ch. J. Palmstrøm, and E. P. A. M. Bakkers, Epitaxy of advanced nanowire quantum devices, Nature (London) **548**, 434 (2017).

[34] Ch. Reeg, D. Loss, and J. Klinovaja, Finite-size effects in a nanowire strongly coupled to a thin superconducting shell, Phys. Rev. B **96**, 125426 (2017).
[35] E. Prada, P. San-Jose, and R. Aguado, Transport spectroscopy of NS nanowire junctions with Majorana fermions, Phys. Rev. B **86**, 180503 (2012).
[36] D. Chevallier and J. Klinovaja, Tomography of Majorana fermions with STM tips, Phys. Rev. B **94**, 035417 (2016).
[37] J. Stenger and T. D. Stanescu, Tunneling conductance in semiconductor-superconductor hybrid structures, arXiv: 1703.02543.
[38] P. G. de Gennes, *Superconductivity of Metals and Alloys* (Addison-Wesley, Boston, 1989).
[39] H. Matsui, T. Sato, T. Takahashi, S.-C. Wang, H.-B. Yang, H. Ding, T. Fujii, T. Watanabe, and A. Matsuda, BCS-Like Bogoliubov Quasiparticles in High-T_c Superconductors Observed by Angle-Resolved Photoemission Spectroscopy, Phys. Rev. Lett. **90**, 217002 (2003).
[40] J. Figgins and D. K. Morr, Differential Conductance and Quantum Interference in Kondo Systems, Phys. Rev. Lett. **104**, 187202 (2010).
[41] J. Tersoff and D. R. Hamann, Theory of the scanning tunneling microscope, Phys. Rev. B **31**, 805 (1985).
[42] J. Klinovaja and D. Loss, Composite Majorana fermion wave functions in nanowires, Phys. Rev. B **86**, 085408 (2012).
[43] W. S. Cole, S. Das Sarma, and T. D. Stanescu, Effects of large induced superconducting gap on semiconductor Majorana nanowires, Phys. Rev. B **92**, 174511 (2015).
[44] Ch.-X. Liu, J. D. Sau, T. D. Stanescu, and S. Das Sarma, Andreev bound states versus Majorana bound states in quantum-dot–nanowire-superconductor hybrid structures: Trivial versus topological zero-bias conductance peaks, Phys. Rev. B **96**, 075161 (2017).
[45] C. L. Kane and E. J. Mele, Z_2 Topological Order and the Quantum Spin Hall Effect, Phys. Rev. Lett. **95**, 146802 (2005).
[46] X.-L. Qi and S.-Ch. Zhang, Topological insulators and superconductors, Rev. Mod. Phys. **83**, 1057 (2011).
[47] P. Zhang and F. Nori, Majorana bound states in a disordered quantum dot chain, New J. Phys. **18**, 043033 (2016).
[48] Y. Oreg, G. Refael, and F. von Oppen, Helical Liquids and Majorana Bound States in Quantum Wires, Phys. Rev. Lett. **105**, 177002 (2010).
[49] Ch. Reeg and D. L. Maslov, Transport signatures of topological superconductivity in a proximity-coupled nanowire, Phys. Rev. B **95**, 205439 (2017).
[50] L. P. Gor'kov and E. I. Rashba, Superconducting 2D System with Lifted Spin Degeneracy: Mixed Singlet-Triplet State, Phys. Rev. Lett. **87**, 037004 (2001).
[51] Ch. Zhang, S. Tewari, R. M. Lutchyn, and S. Das Sarma, $p_x + ip_y$ Superfluid from S-Wave Interactions of Fermionic Cold Atoms, Phys. Rev. Lett. **101**, 160401 (2008).
[52] J. Alicea, Majorana fermions in a tunable semiconductor device, Phys. Rev. B **81**, 125318 (2010).
[53] K. Seo, L. Han, and C. A. R. Sá de Melo, Topological phase transitions in ultracold Fermi superfluids: The evolution from Bardeen-Cooper-Schrieffer to Bose-Einstein-condensate superfluids under artificial spin-orbit fields, Phys. Rev. A **85**, 033601 (2012).
[54] T. Yu and M. W. Wu, Gapped triplet p-wave superconductivity in strong spin-orbit-coupled semiconductor quantum wells in proximity to s-wave superconductor, Phys. Rev. B **93**, 195308 (2016).
[55] M. Gibertini, F. Taddei, M. Polini, and R. Fazio, Local density of states in metal-topological superconductor hybrid systems, Phys. Rev. B **85**, 144525 (2012).
[56] J. Liu, A. C. Potter, K. T. Law, and P. A. Lee, Zero-Bias Peaks in the Tunneling Conductance of Spin-Orbit-Coupled Superconducting Wires with and without Majorana End States, Phys. Rev. Lett. **109**, 267002 (2012).
[57] B. van Heck, R. M. Lutchyn, and L. I. Glazman, Conductance of a proximitized nanowire in the Coulomb blockade regime, Phys. Rev. B **93**, 235431 (2016).
[58] Ch.-X. Liu, J. D. Sau, and S. Das Sarma, Role of dissipation in realistic Majorana nanowires, Phys. Rev. B **95**, 054502 (2017).
[59] J. Danon, E. B. Hansen, and K. Flensberg, Conductance spectroscopy on Majorana wires and the inverse proximity effect, Phys. Rev. B **96**, 125420 (2017).
[60] P. Devillard, D. Chevallier, and M. Albert, Fingerprints of majorana fermions in current-correlation measurements from a superconducting tunnel microscope, Phys. Rev. B **96**, 115413 (2017).
[61] Ch.-X. Liu, F. Setiawan, J. D. Sau, and S. Das Sarma, Phenomenology of the soft gap, zero-bias peak, and zero-mode splitting in ideal Majorana nanowires, Phys. Rev. B **96**, 054520 (2017).
[62] F. Setiawan, Ch.-X. Liu, J. D. Sau, and S. Das Sarma, Electron temperature and tunnel coupling dependence of zero-bias and almost-zero-bias conductance peaks in Majorana nanowires, arXiv:1708.09039.
[63] E. Prada, R. Aguado, and P. San-Jose, Measuring Majorana nonlocality and spin structure with a quantum dot, Phys. Rev. B **96**, 085418 (2017).
[64] A. C. Potter and P. A. Lee, Multichannel Generalization of Kitaev's Majorana End States and a Practical Route to Realize Them in Thin Films, Phys. Rev. Lett. **105**, 227003 (2010).
[65] S. Das Sarma, J. D. Sau, and T. D. Stanescu, Splitting of the zero-bias conductance peak as smoking gun evidence for the existence of the Majorana mode in a superconductor-semiconductor nanowire, Phys. Rev. B **86**, 220506 (2012).
[66] X.-J. Liu, Soliton-induced Majorana fermions in a one-dimensional atomic topological superfluid, Phys. Rev. A **91**, 023610 (2015).
[67] H. Zhang, Ö. Gül, S. Conesa-Boj, M. P. Nowak, M. Wimmer, K. Zuo, V. Mourik, F. K. de Vries, J. van Veen, M. W. A. de Moor, J. D. S. Bommer, D. J. van Woerkom, D. Car, S. R. Plissard, E. P. A. M. Bakkers, M. Quintero-Pérez, M. C. Cassidy, S. Koelling, S. Goswami, K. Watanabe, T. Taniguchi, and L. P. Kouwenhoven, Ballistic superconductivity in semiconductor nanowires, Nat. Commun. **8**, 16025 (2017).
[68] Ch. Moore, T. D. Stanescu, and S. Tewari, Majorana bound states in non-homogeneous semiconductor nanowires, arXiv:1611.07058.
[69] W. S. Cole, J. D. Sau, and S. Das Sarma, Proximity effect and Majorana bound states in clean semiconductor nanowires coupled to disordered superconductors, Phys. Rev. B **94**, 140505 (2016).
[70] S. S. Hegde and S. Vishveshwara, Majorana wave-function oscillations, fermion parity switches, and disorder in Kitaev chains, Phys. Rev. B **94**, 115166 (2016).

[71] O. A. Awoga, K. Björnson, and A. M. Black-Schaffer, Disorder robustness and protection of Majorana bound states in ferromagnetic chains on conventional superconductors, Phys. Rev. B **95**, 184511 (2017).

[72] X.-J. Liu and P. D. Drummond, Manipulating Majorana fermions in one-dimensional spin-orbit-coupled atomic Fermi gases, Phys. Rev. A **86**, 035602 (2012).

[73] Y. Xu, L. Mao, B. Wu, and Ch. Zhang, Dark Solitons with Majorana Fermions in Spin-Orbit-Coupled Fermi Gases, Phys. Rev. Lett. **113**, 130404 (2014).

[74] M. M. Maśka, A. Gorczyca-Goraj, J. Tworzydło, and T. Domański, Majorana quasiparticles of an inhomogeneous Rashba chain, Phys. Rev. B **95**, 045429 (2017).

[75] A. Ptok, A. Cichy, and T. Domański, Quantum engineering of Majorana quasiparticles in one-dimensional optical lattices, arXiv:1706.04155.

[76] J.-D. Pillet, C. H. L. Quay, P. Morfin, C. Bena, A. L. Yeyati, and P. Joyez, Andreev bound states in supercurrent-carrying carbon nanotubes revealed, Nat. Phys. **6**, 965 (2010).

[77] T. Dirks, T. L. Hughes, S. Lal, B. Uchoa, Y.-F. Chen, C. Chialvo, P. M. Goldbart, and N. Mason, Transport through Andreev bound states in a graphene quantum dot, Nat. Phys. **7**, 386 (2011).

[78] J.-D. Pillet, P. Joyez, R. Žitko, and M. F. Goffman, Tunneling spectroscopy of a single quantum dot coupled to a superconductor: From Kondo ridge to Andreev bound states, Phys. Rev. B **88**, 045101 (2013).

[79] E. J. H. Lee, X. Jiang, M. Houzet, R. Aguado, Ch. M. Lieber, and S. De Franceschi, Spin-resolved Andreev levels and parity crossings in hybrid superconductor-semiconductor nanostructures, Nat. Nanotech. **9**, 79 (2014).

[80] J. Barański and T. Domański, In-gap states of a quantum dot coupled between a normal and a superconducting lead, J. Phys.: Condens. Matter **25**, 435305 (2013).

[81] P. Szumniak, D. Chevallier, D. Loss, and J. Klinovaja, Spin and charge signatures of topological superconductivity in Rashba nanowires, Phys. Rev. B **96**, 041401 (2017).

[82] S. Folsch, J. Martinez-Blanco, J. Yang, K. Kanisawa, and S. C. Erwin, Quantum dots with single-atom precision, Nat. Nanotech. **9**, 505 (2014).

[83] J. Cayao, E. Prada, P. San-Jose, and R. Aguado, SNS junctions in nanowires with spin-orbit coupling: Role of confinement and helicity on the subgap spectrum, Phys. Rev. B **91**, 024514 (2015).

[84] J. J. He, T. K. Ng, P. A. Lee, and K. T. Law, Selective Equal-Spin Andreev Reflections Induced by Majorana Fermions, Phys. Rev. Lett. **112**, 037001 (2014).

[85] L.-H. Hu, Ch. Li, D.-H. Xu, Y. Zhou, and F.-Ch. Zhang, Theory of spin-selective Andreev reflection in the vortex core of a topological superconductor, Phys. Rev. B **94**, 224501 (2016).

[86] H.-H. Sun, K.-W. Zhang, L.-H. Hu, Ch. Li, G.-Y. Wang, H.-Y. Ma, Z.-A. Xu, Ch.-L. Gao, D.-D. Guan, Y.-Y. Li, C. Liu, D. Qian, Y. Zhou, L. Fu, S.-Ch. Li, F.-Ch. Zhang, and J.-F. Jia, Majorana Zero Mode Detected with Spin Selective Andreev Reflection in the Vortex of a Topological Superconductor, Phys. Rev. Lett. **116**, 257003 (2016).

[87] R. Chirla and C. P. Moca, Fingerprints of Majorana fermions in spin-resolved subgap spectroscopy, Phys. Rev. B **94**, 045405 (2016).

[88] M. M. Maśka and T. Domański, Spin-polarized Andreev tunneling through the Rashba chain, arXiv:1706.01468.

[89] J.-P. Xu, M.-X. Wang, Z. L. Liu, J.-F. Ge, X. Yang, C. Liu, Z. A. Xu, D. Guan, Ch. L. Gao, D. Qian, Y. Liu, Q.-H. Wang, F.-Ch. Zhang, Q.-K. Xue, and J.-F. Jia, Experimental Detection of a Majorana Mode in the Core of a Magnetic Vortex Inside a Topological Insulator-Superconductor $Bi_2Te_3/NbSe_2$ Heterostructure, Phys. Rev. Lett. **114**, 017001 (2015).

[90] H. Li, T. Zhou, J. He, H.-W. Wang, H. Zhang, H.-Ch. Liu, Y. Yi, Ch. Wu, K. T. Law, H. He, and J. Wang, Origin of bias-independent conductance plateaus and zero-bias conductance peaks in $Bi_2Se_3/NbSe_2$ hybrid structures, Phys. Rev. B **96**, 075107 (2017).

[91] S. Jeon, Y. Xie, J. Li, Z. Wang, B. A. Bernevig, and A. Yazdani, Distinguishing a Majorana zero mode using spin-resolved measurements, Science **358**, 772 (2017).

[92] J. Li, S. Jeon, Y. Xie, A. Yazdani, and B. A. Bernevig, The Majorana spin in magnetic atomic chain systems, arXiv:1709.05967.

[93] K. Björnson and A. M. Black-Schaffer, Probing chiral edge states in topological superconductors through spin-polarized local density of state measurements, arXiv:1709.09061.

[94] A. Yamakage and M. Sato, Interference of Majorana fermions in NS junctions, Phys. E **55**, 13 (2014).

[95] J. Barański, A. Kobiałka, and T. Domański, Spin-sensitive interference due to Majorana state on the interface between normal and superconducting leads, J. Phys.: Condens. Matter **29**, 075603 (2017).

[96] F. Setiawan, W. S. Cole, J. D. Sau, and S. Das Sarma, Conductance spectroscopy of nontopological-topological superconductor junctions, Phys. Rev. B **95**, 020501 (2017).

[97] S. Hoffman, D. Chevallier, D. Loss, and J. Klinovaja, Spin-dependent coupling between quantum dots and topological quantum wires, Phys. Rev. B **96**, 045440 (2017).

[98] L. H. Guessi, F. A. Dessotti, Y. Marques, L. S. Ricco, G. M. Pereira, P. Menegasso, M. de Souza, and A. C. Seridonio, Encrypting Majorana fermion qubits as bound states in the continuum, Phys. Rev. B **96**, 041114 (2017).

[99] S. Hoffman, C. Schrade, J. Klinovaja, and D. Loss, Universal quantum computation with hybrid spin-majorana qubits, Phys. Rev. B **94**, 045316 (2016).

[100] D. Chevallier, P. Szumniak, S. Hoffman, D. Loss, and J. Klinovaja, Topological phase detection in Rashba nanowires with a quantum dot, arXiv:1710.05576.